Two-dimensional density and density fluctuation diagnostic for the edge plasma in fusion devices

S. Zoletnik, G. Petravich, and A. Bencze
KFKI-Research Institute for Particle and Nuclear Physics, P.O.B. 49, H-1525 Budapest, Hungary

M. Berta
Budapest University of Technology and Economics, Institute of Nuclear Techniques 1111 Budapest, Műegyetem rkp. 9 and Széchenyi István University, Department of Physics 9026 Győr, Egyetem tér 1

S. Fiedler, K. McCormick, and J. Schweinzer
Max-Planck Institut für Plasmaphysik, Association Euratom, Boltzmannstr. 2, D-85748 Garching bei München

(Received 3 February 2005; accepted 16 May 2005; published online 23 June 2005)

A technique is described for the two-dimensional measurement of electron density profile and fluctuations in edge regions of magnetically confined fusion plasmas. The method is based on existing lithium beam beam emission spectroscopy technique, two-dimensional resolution is achieved by electrostatically scanning the beam. If scanning is performed faster than the lifetime of the turbulent structures in the plasma, the diagnostic is capable of measuring the structure of electron density fluctuations as well. The beam strength of currently available beams makes the detection of single fluctuation events impossible, but the full two-dimensional spatial structure of correlations can still be determined. The article describes the technique and fast beam deflection tests up to 250 kHz. The capabilities of such a diagnostic for fluctuation measurement are explored by simulating measurement signals. Measurement of both the two-dimensional density profile, fluctuation correlation function and poloidal flow velocity are demonstrated at the Wendelstein 7-AS stellarator. The shape of the density profile, the radial and poloidal correlation lengths and the flow velocity are in agreement with expectations and previous Langmuir probe measurement. © *2005 American Institute of Physics.* [DOI: 10.1063/1.1947727]

I. INTRODUCTION

Beam emission spectroscopy (BES) using both thermal[1] and accelerated[2–4] neutral particle beams became a routine technique for the determination of electron density profiles in fusion plasmas. The method is based on the fact that light emission from the neutral beam penetrating the plasma depends on the plasma parameters. In the case of certain beam species (e.g., Li, Na) the sensitivity on the electron temperature is small, thus the electron density profile primarily determines the beam light emission. In this article we shall concentrate on such beams. Although the light intensity is not a local function of the electron density, numerical techniques were developed[3] which can determine the electron density distribution along the beam if the light emission distribution is detected with appropriate spatial resolution.

BES techniques have also been used for the measurement of electron density fluctuations,[4–8] which are believed to be connected to anomalous plasma transport. As investigations in the scrape-off layer (SOL) and edge plasma[9–11] indicated strong radially dependent poloidal flows, some of the BES fluctuation measurements aimed at achieving a two-dimensional (2D) radial-poloidal resolution by utilizing an extended beam[5,12] or multiple beams[13] and tangential (i.e., $B_{\|}$) observation. The radial and the poloidal correlation length were indeed measured both in the core[5] and the SOL and edge[13] of a tokamak plasma. However, a wide neutral beam and appropriate tangential observation are not always easily achievable.

On the Wendelstein 7-AS (W7-AS) stellarator detailed measurements were done[14] with an accelerated Li beam.[2] This diagnostic has a large number of measuring channels (28) along the beam which covers most of the minor radius of the plasma and the SOL. Depending on the plasma density, either the outer 70% (at low density) or the outer 10% (at the highest densities) of the plasma minor radius can be analyzed for fluctuations. Although this diagnostic provided a detailed picture of the radial correlation length and the correlation times of fluctuations, the interpretation of the results is hindered by the lack of information on the poloidal flow velocity and correlation length.

The aim of this article is to describe an extension of the W7-AS Li-beam diagnostic[2] to two dimensions both for electron density profile and fluctuation measurement. The setup keeps the basic geometrical arrangement intact, thus no special view angles are needed. The general concept of a two-dimensional setup is described and discussed in Sec. II. The capabilities of such a system are explored in Sec. III. The technical details of the Wendelstein 7-AS setup and detailed testing of high-frequency beam deflection are presented in Sec. IV. Some results from the diagnostic are shown in Sec. V.

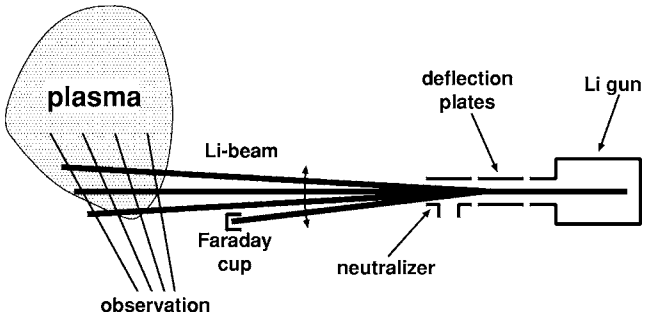

FIG. 1. Experimental setup for two-dimensional measurement using a neutral Li beam.

II. TWO-DIMENSIONAL EXTENSION OF A STANDARD BES DIAGNOSTIC

A general scheme of the experimental setup is shown in Fig. 1. We consider the case of a standard accelerated Li-beam diagnostic. An ionized lithium beam is formed in the beam gun which consists of a heated solid-state ion emitter and ion optics. The energy of the beam is typically in the 30–60 keV range, the beam current on the cathode is up to 2.5 mA. The ionized beam passes between two deflection plates which produce an electric field perpendicular to the beam velocity. By adjusting the polarity and magnitude of this field the beam can be moved in a plane defined by the undeflected beam and the electric field vector. In the neutralizing cell the ionized beam passes through sodium (or lithium) vapor and gets neutralized via charge exchange. The neutralizer should be placed as close to the deflection plates as possible to keep beam movement inside the neutralizer at a minimum. The neutral beam leaving the neutralizer travels in the direction which was set by the electric field between the deflection plates. A Faraday cup can be placed in a position to which the beam can be deflected but does not hinder beam scan for the measurement.

This Faraday cup serves two purposes. First it can be used for beam monitoring, and second the beam can be removed from the plasma by deflecting it into the Faraday cup. Regularly doing so the background plasma radiation can be measured in the detection system and corrected for in the data evaluation. Considering the faint light from the neutral beam, this can be crucial in the case of high density plasma discharges.

The detection system measures the radiation of the neutral Li beam atoms emitted at the 670.8 nm resonance transition along multiple lines of sight. Each measuring chord should be wide enough perpendicular to the beam so it sees the whole width of the beam. Along the beam the individual measuring channels collect light only from a limited range, typically 0.5–1 cm. The basic idea of the two-dimensional measurement is the fact that the light detected in a measurement channel originates from the crossing point of the beam and the line of sight. This way, if the beam is scanned up and down in the plane defined by the lines of sight and the center point of the deflection plates, the measurement points are also moving up and down along the lines of sight. Measuring the beam light profile at a given beam position, one can reconstruct the electron density profile along the beam line in question. Doing a series of measurements at a set of different beam positions, the whole two-dimensional density profile can be recovered, albeit not on a rectangular grid of points.

It has to be noted that the beam movement should be stepwise and not continuous because some time is needed for recording the emitted light at a beam position. Such a stepwise scanning setup can be considered as a system of "virtual beams." These beams exist at a certain position only for a certain fraction of time.

The optical system is equipped with interference filters to select the 670.8 nm wavelength of the lithium $2p$-$2s$ transition. This can be done either using a single wide band interference filter which can pass through the differently Doppler shifted light at different measuring channels or by individual narrow band filters tailored for the individual channels. It should be noted that during the beam scan the observation angle changes slightly which should be taken into consideration in the design. In the case of the W7-AS test setup a single wide band interference filter was used in which case the change in observation angle had no effect.

The achievable spatial resolution of the scanning beam measurement is determined by the resolution along the beam and the beam width which are both about 1–1.5 cm. The deflection step size (distance of virtual beams) can be taken equal to the beam width. Assuming some reasonable scan range, e.g. ±10 cm in the plasma, one needs to measure at 12 virtual beam positions. The time resolution of such a two-dimensional measurement can be assessed by taking into account the minimum time needed for a light profile measurement. (Provided the beam can be moved between virtual beam positions in a much shorter time.) The time needed for a profile measurement is determined by the beam light intensity and it is about 0.2 ms for the W7-AS Li-beam diagnostic. In addition to the 12 measurements an extra time slot is needed for the measurement of the background (not Li $2p$) light when the beam is deflected into the Faraday cup. As a result the total measurement time is about 2.5 ms. This is appropriate for most cases, but can be inadequate in the case of transient phenomena, e.g., edge localized modes (ELMs). However, if the perpendicular resolution is reduced to a few positions (which can be arbitrarily placed), the temporal resolution can be as good as 1 ms. A further complication can arise if the background light detected by the optics is changing on the millisecond time scale, as is typical for ELMs.[15] This case will be considered later.

If the diagnostic is to be used for the investigation of density fluctuations in the plasma, then the temporal resolution should be compared to the autocorrelation time of the fluctuations. This is typically in the 10–100 μs range for the SOL and the edge plasma. Typical autocorrelation functions of fluctuations in the Wendelstein 7-AS plasma are shown in Fig. 2.[14]

As one can see, the correlation time of fluctuations is shorter than the time needed for the measurement of a light profile ($\approx$0.2 ms) thus the two-dimensional structure cannot be measured with the scanning BES diagnostic. However, correlation functions can still be measured if the beam can be moved between two virtual beam positions in a time much shorter than the correlation time of fluctuations. As an ex-

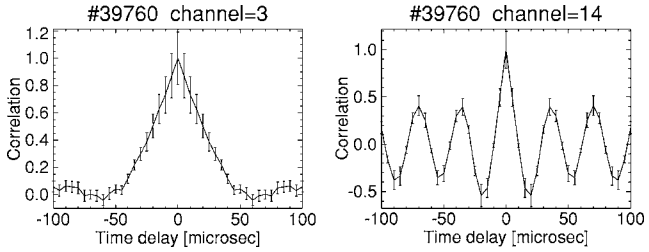

FIG. 2. Autocorrelation functions of Li-beam light fluctuations measured in the SOL (left) and in the edge plasma (right) of W7-AS.

ample a possible implementation for a nine-point correlation measurement is explained in Fig. 3. Here the beam is assumed to be moved from one position to another in zero time. The beam is moved over all nine positions in cycles. One cycle (between the long dashed lines) consists of nine time intervals each of T time long. T is selected in a way to be shorter than the correlation time of the fluctuation, e.g., it can be set to 5 μs. Each T time long interval has two parts, (a) and (b). In (a) the beam is in the reference position, in (b) it is moved to one of the nine positions (including the reference). If the detection system has a time constant much shorter than T then the correlation function between the reference position ($i=0$) and any of the other eight positions ($i=1\ldots8$) with time lag $\tau_j=T/2+jT$ can be calculated as

$$C_i(T/2+jT)=\sum_{\ell}\int_{\ell 9T+iT+T/2}^{\ell 9T+iT+T} S(t-T/2-jT)S(t)dt, \qquad i=0\ldots8. \tag{2.1}$$

Here the sum over ℓ performs summing up the correlation function over many $9T$ time long deflection periods to reach sufficient signal statistics. As one can see, correlation functions can be calculated with T time resolution at discrete τ time lags. The above considerations were done only for calculating correlations within one detection channel, that is, between spatial points aligned along one line of sight. Correlations between different detection channels can be calculated exactly the same way and a full three-dimensional (3D) (radial-poloidal-time) correlation function can be built up this way on a mash of points $x=x_k, y=y_j, \tau=iT+T/2$. Here k,j,i counts over detection channels, virtual beams and sampling time lags, respectively.

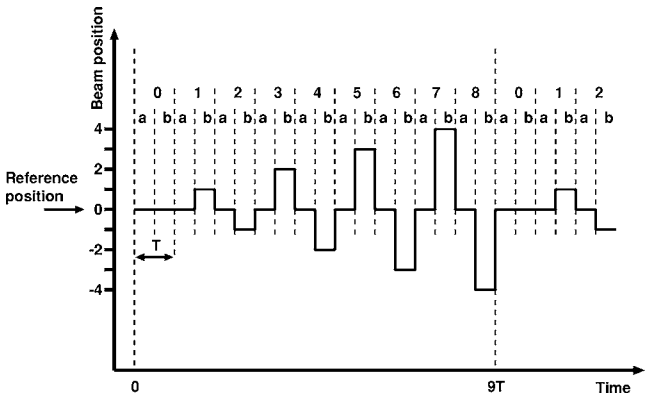

FIG. 3. Beam position vs time for a nine-point correlation measurement.

The measurement time devoted to the determination of one correlation function is $1/(2N)$ part of the total measurement time, where N is the number of beam positions measured. For the W7-AS setup the minimum integration time needed for the determination of correlation functions is 10 ms,[14] thus a two-point measurement can be done in about 40 ms. Even a nine point measurement should be possible using a 180 ms flattop part of the discharge. It has to be noted that correlations are always calculated *relative* to a reference position. The correlation between other positions cannot be calculated this way. On the other hand, the deflection to different virtual beam positions need not necessarily be done in the way shown in Fig. 3, but it can also be done as independent two-position measurements by keeping the reference position fixed and changing the deflected position. These two-point measurements can even be performed in different plasma discharges by changing the amount of beam deflection on a shot-to-shot basis.

For fluctuation measurement the necessary resolution and maximum deflection of the beam in the plasma are determined by the spatial correlation length of the fluctuations. In the SOL both the poloidal wavelength and correlation length were found to be less than 5 cm,[9] thus a maximum beam deflection of ±5 cm in the plasma is adequate. As the beam width is typically 1.5 cm, 6–8 measurement positions would be necessary.

Let us assess the necessary parameters of such a scanning beam setup. If the distance of the deflection plates from the observation volume is L and the poloidal beam movement needed in the plasma is $\pm s$, the beam needs to be deflected by an angle of $s/L=v_\perp/v_b$. Here v_b is the beam velocity and $v_\perp$ is the beam velocity perpendicular to the original beam path. If the deflection plates have length ℓ and separation d and the voltage between the two deflection plates is U, then for an E_b energy beam we get

$$v_\perp=\frac{e}{m}\frac{U}{d}\frac{\ell}{v_b}, \quad s=\frac{e}{m}\frac{U}{d}\frac{\ell}{v_b^2}L=\frac{eU}{2E_b}\frac{\ell}{d}L \tag{2.2}$$

(e is the electron charge and m is the ion mass.) The typical width of the Li beam is 1.5 cm, thus $d=4$ cm is a reasonable choice. To keep beam movement at a minimum in the neutralization cell $\ell \ll L$ should be fulfilled. To keep the beam focused $\ell > d$ is also desirable. Choosing $\ell=10$ cm and $U=1000$ V one gets $s/L=0.025$ for a 48 keV Li beam. This means that for a reasonable perpendicular measurement range of ±5 cm, $L=2$ m is necessary. This is approximately the neutralizer-plasma distance in the W7-AS setup.

The minimum time needed to move the beam from one position to another is determined by the transit time of the ions between the deflection plates

$$\tau_t=\frac{\ell}{v_b}. \tag{2.3}$$

For 10 cm plate length and 48 keV beam energy τ_t is somewhat less than 100 ns. This time is indeed about two orders of magnitude shorter than the correlation time of the density fluctuations, thus the setup explained in Fig. 3 is possible and experimental evidence will be given below.

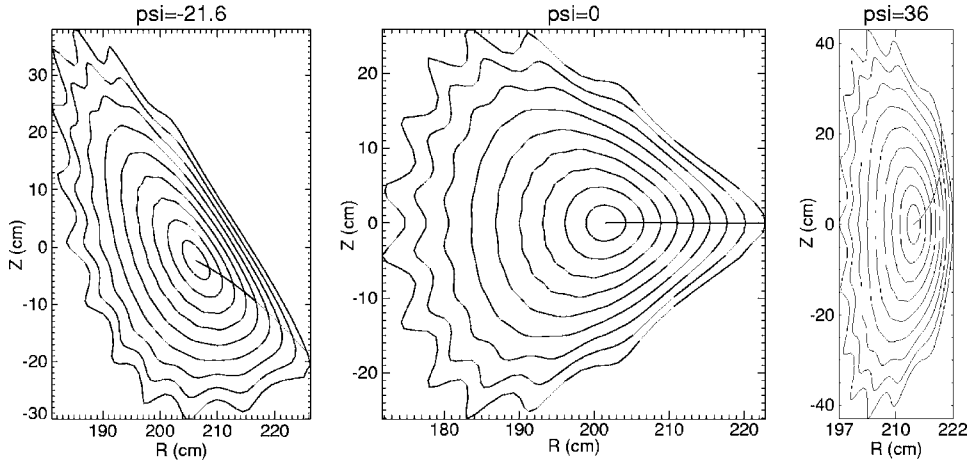

FIG. 4. The $\varphi=0$ lines in various sections of the Wendelstein 7-AS stellarator.

The fast deflection scheme described above can also be used for the measurement of the background light intensity in the measurement channels. If one of the beam positions is the Faraday cup, then that time period can be used for determination of the background light intensity. This way the light profiles can be corrected for the background light even in cases when the background light intensity changes on a sub-ms time scale.

III. SIMULATED FLUCTUATION MEASUREMENTS

In Sec. II we have shown that determination of the full three-dimensional correlation function is possible using a scanning BES setup, provided the light emitted by the beam is proportional to the local plasma electron density. However, this is fulfilled only approximately and in a general case special techniques are needed to reconstruct the correct correlation function of electron density fluctuations from the measured correlation function of beam light fluctuations.[8] As a first attempt to use the two-dimensional method, we do not aim at developing a reconstruction method for the exact density correlation function but we investigate the applicability of the method to real cases under moderate beam attenuation conditions. The aim of this section is to explore to what extent poloidal flow velocity and correlation function can be analyzed from the measured two-dimensional beam light correlation functions.

In order to get information about the effect of Li-beam atomic physics on the determination of the poloidal velocity and correlation functions, we have done a simulation of density fluctuation signal in real 3D stellarator geometry. In this section we present some technical details of such a simulation and then we discuss simulation results.

A. Simulated perturbations

As fluctuation measurements on various machines show $k_{\|}\approx 0$, the structures are simulated in *magnetic flux coordinates* (straight field line coordinates), following the magnetic field lines. Gaussian shapes are considered with different widths in radial, poloidal and $B_{\|}$ direction.

The three coordinates of the flux coordinate system are defined as follows. The shape of the poloidal flux contours and magnetic field lines is taken from an equilibrium reconstruction of a discharge. The ψ coordinate is taken equal to the toroidal angle. The R_{eff} radial coordinate labels the magnetic surfaces. The φ poloidal angle labels the magnetic field lines on a magnetic surface (*field line label*), therefore $\varphi=\mathrm{const}$, $R_{\mathrm{eff}}=\mathrm{const}$ marks a single field line φ; is set to 0 along a horizontal line starting from the magnetic axis to the outer edge of the plasma in a fixed $\psi=\psi_0$ section, as shown in Fig. 4. The scale of φ is defined in a way that the flux in a $d\varphi\times dR_{\mathrm{eff}}$ box is constant on a flux contour.

As we need to calculate the effect of the perturbations in the (R,Z,ψ) cylindrical coordinate system, the mapping between this and the $(R_{\mathrm{eff}},\phi,\psi)$ coordinate system constitutes the essence of the simulation. For a given (R,Z,ψ) point R_{eff} is calculated from the local flux contours at ψ, while φ is determined by following the magnetic field line around the torus to ψ_0.

Mapping along the field lines is not done explicitly but it is based on interpolation in a table of pre-calculated field line mapping data. This method ensures short calculation times and flexibility to use magnetic geometry from different machines and discharges. The results shown in this article were calculated using mapping data from the TRANS code, which represents a finite beta equilibrium reconstruction of a W7-AS discharge.

The above described $(R,Z,\psi)\rightarrow(R_{\mathrm{eff}},\varphi,\psi)$ transformation provides multiple φ values for one point as field line tracing can be done in either positive or negative ψ direction and it can be continued over many toroidal turns. This is indeed necessary if the structures have a length comparable to the major circumference of the torus, as observed experimentally.[16] This problem of multivalued coordinates is handled by keeping a finite number of these mappings with appropriate $\psi=\psi\pm n\cdot 2\pi,(n=0,1,\ldots)$ coordinates as shown by $P_0,P_1^{\pm},\ldots,P_i^{\pm}$ in Fig. 5.

The simulated turbulence structures are generated with random φ_0,ψ_0 center points in the $\psi_0,\varphi_0\in[0,2\pi]$ range but observation points are enabled outside of this ψ range as well. This corresponds to the fact that the "tail" of a structure might be seen by the measurement after several toroidal turns. In the actual simulation the value of the perturbation is calculated at every mapped measurement point and the largest value is kept as the actual measurement signal. If the perturbation is sufficiently localized poloidally only one of

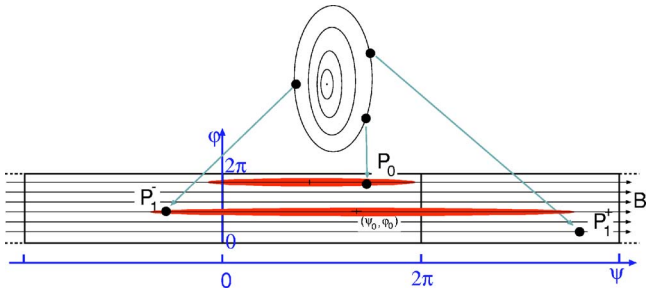

FIG. 5. Measurement points and Gaussian structures in an R_{eff}=const surface in the (ψ,φ) coordinate system. The $P_i^{\pm}$ multiple virtual measurement points all belong to a single real measurement point in the (R,Z,ψ) physical coorrdinate system. (Only points P_0, and $P_1^{\pm}$ are shown.)

these "virtual measurement values" will be different from zero. This approach fails if the rotational transform is close to a low-order rational so as the structures map on them-self along a field line. This case is excluded from the current version of the simulation.

The shape of the perturbations is described by a Gaussian with fixed (but different) widths w_R, w_φ, w_ψ along R_{eff}, φ and ψ, respectively. The A_0 amplitude is kept constant. The temporal behavior is also taken to be Gaussian with a certain lifetime and they are moved along φ with a given v_φ velocity

$$A(R_{\mathrm{eff}},\varphi,\psi,t) = A_0 \exp\left\{ -\frac{(R_{\mathrm{eff}}-R_{\mathrm{eff}}^0)^2}{2w_R^2} - \frac{(\varphi + v_\varphi(R_{\mathrm{eff}})t-\varphi_0)^2}{2w_\varphi^2} - \frac{(\psi-\psi_0)^2}{2w_\psi^2} - \frac{(t-t_0)^2}{2w_t^2} \right\}. \quad (3.1)$$

(Toroidal flow is not considered because in the nonaxisymmetric W7-AS machine the dominant flow velocity is expected to be poloidal.) To be able to base the simulation on experimental data, the flow velocity is not given by v_φ but by the v_p poloidal velocity in the physical R,Z coordinate system at $\psi_0,\varphi_0=0$, where the poloidal velocity is vertical. The flow velocity in the transformed coordinates is calculated as $v_\varphi=(\partial\varphi/\partial Z)v_p$. Taking a $v_p(R)$ velocity profile we arrive at $v_\varphi(R_{\mathrm{eff}})$. Although v_φ is independent of φ, the flow velocity in real physical space is strongly dependent on the poloidal location due to flux compression.

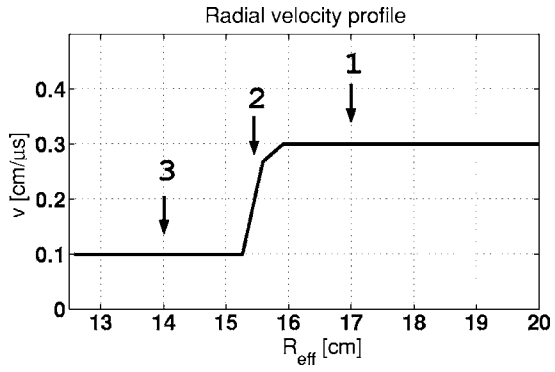

FIG. 6. Simulated radial profile of the poloidal flow velocity of turbulent structures. The horizontal coordinate shows effective radius (flux surface label), the beam travels from right to left.

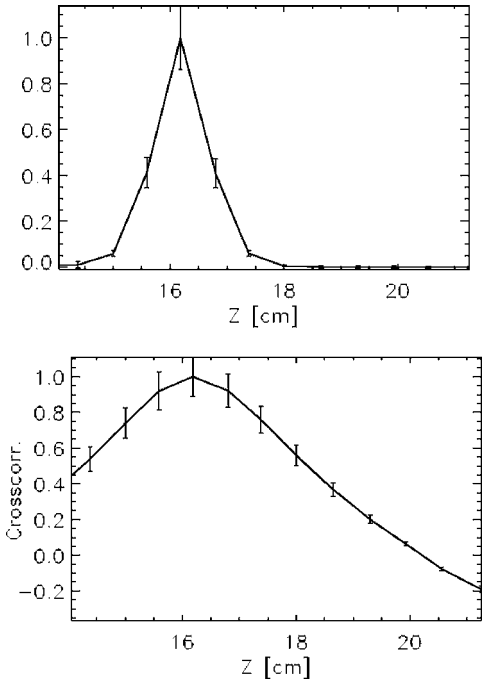

FIG. 7. Normalized correlation amplitude along the beam (reference position at Z=16 cm)—density fluctuations (top), light fluctuations (bottom). Z measures distance along the beam, the beam travels from left to right.

B. Simulation results

Simulations of the fluctuation signal which would be measured by a quasi two-dimensional Li-beam diagnostic were done at seven different voltages applied onto the deflection plates (0, ±50, ±100, ±150, ±200, ±250, and ±300 V), in a two virtual beam configuration: the beam is periodically moved between the reference position (0 V deflection) and one of the deflected positions or the reference position. The period time was set to T=4 μs, while the sampling time was 0.4 μs. Different deflections are simulated in separate runs. This geometrical setup corresponds to the real implementation of the diagnostic as it will be described in the next section.

$2\cdot10^4$ turbulent events with a lifetime of w_t=10 μs, radial and poloidal width of 2 cm and a toroidal elongation of 1/4 of the toroidal circumference of the stellarator were generated with uniformly distributed center points in the plasma. To calculate the beam light perturbation resulting from these density perturbations, we applied an atomic physics model[3] describing the connection between the plasma density profile and light emission from the neutral Li beam. For the beam energy 48 keV was assumed. The atoms in such a beam travel through the observation volume in about 0.1 μs, which is considerably less than the characteristic time scale of the density perturbations. This way the instantaneous light emission profile was calculated from the density profile along the actual position of the beam. The effect of the density structures on the light profile was taken into account assuming linear but nonlocal response as described in Ref. 8. For different beam positions different transfer functions were

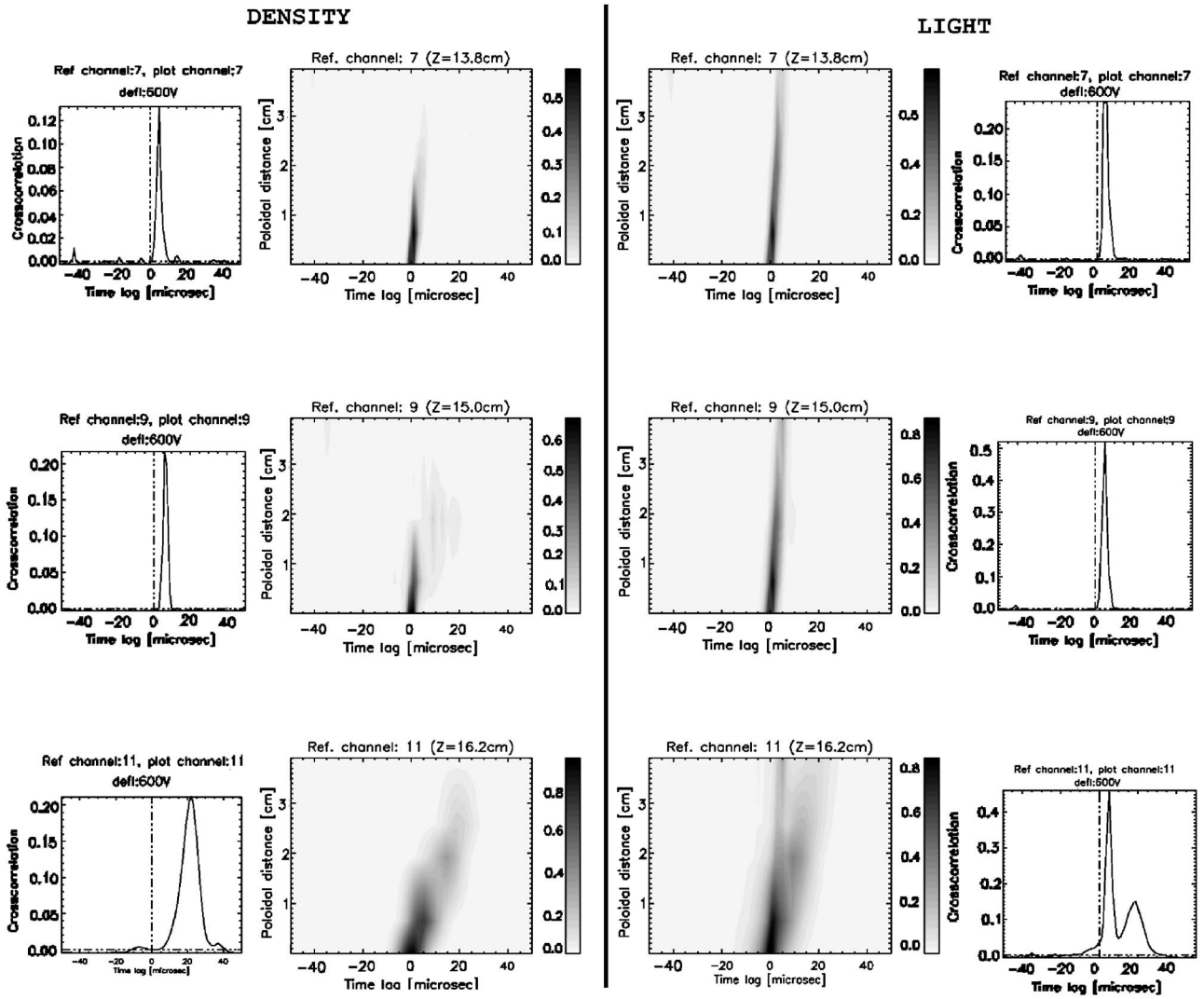

FIG. 8. The plots of the figure show the cross correlation of density fluctuations (left) and light fluctuations (right) along a flux surface at different radial positions in the plasma. On the gray scale plots the horizontal coordinate is time lag, vertical is distance along the flux surface. The smaller plots next to these show horizontal cuts at about 3 cm poloidal distance. Different rows correspond to different R_{eff} positions; the same locations are marked in Fig. 6.

used as calculated from the actual density profile along the beam. The density and temperature profiles for the calculation of the transfer functions were taken from a real experiment as described in the next section.

In the above linear approximation the amplitude of the density fluctuation does not effect the shape of the light profile response or its correlation function, therefore the amplitude of the simulated turbulence events is not relevant. Our simulation is applicable to the case where either the fluctuation amplitude is small (typically $<10\%$) or the absolute magnitude of the plasma density is low, so as beam attenuation does not play a role. In an actual experiment the first condition is fulfilled in the edge and core plasma, while the second condition is applicable to the scrape-off layer. This way this linear approximation is applicable along the wide diagnostic beam.

It is well known that the detected light intensity is not a strictly local function of the plasma electron density. The finite lifetime of excited atomic states causes some spatial integration, while ionization generates a decrease of beam light towards the plasma center. The present simulation is devoted to the clarification of the role of such effects on the capability of flow velocity and poloidal correlation determination from cross-correlation technique. The question of radial correlation reconstruction was studied in detail in Ref. 8.

For our simulation we have used step function as velocity profile as shown in Fig. 6. This is considered to be the best way of demonstrating the effect of beam smearing.

The first and very clear effect can be shown in Fig. 7. Due to the finite lifetime of the exited states of the Li atom, the information about the plasma state is carried inward a couple of cm along the beam. A clear and substantial widening of the cross-correlation structure can be observed.

Since the direction of the beam velocity is not perpendicular to the poloidal direction (see Fig. 12.) a smearing in the poloidal correlations is also expected. Additionally, the beam will carry on the poloidal correlation information for a while, therefore even the location of maxima in the poloidal correlation functions can be effected. These effects are demonstrated in Fig. 8. This figure plots the spatio-temporal correlation function along a flux surface at different positions in the plasma. To obtain correlations along the flux surfaces the

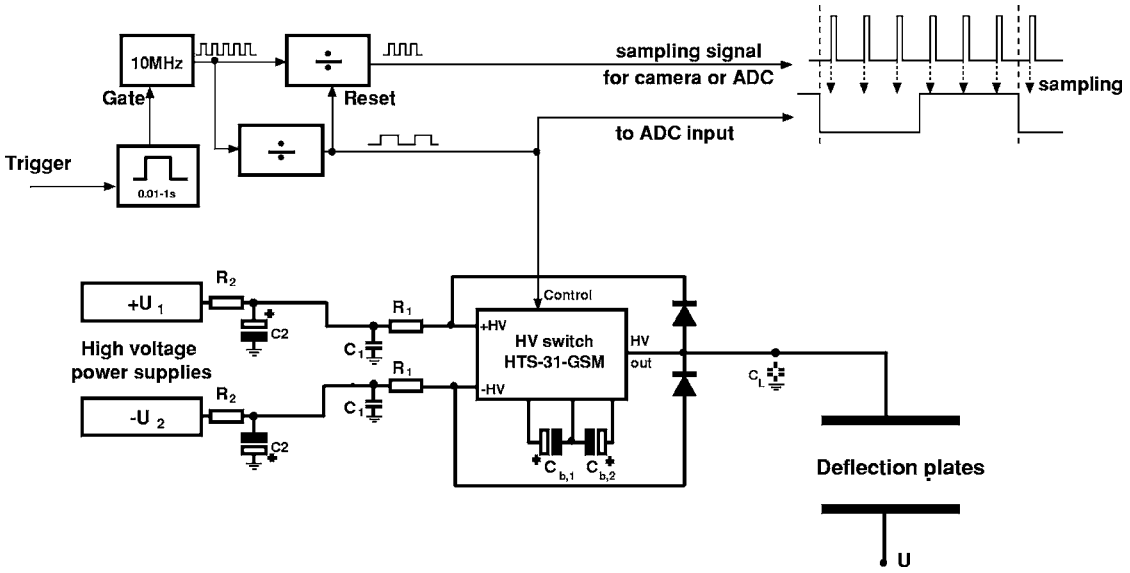

FIG. 9. Electrical connection of the high voltage switch and control circuitry. For test measurements only one deflection plate was driven with this circuitry. In plasma measurements both deflection plates were driven in opposite phase by two identical circuits.

correlation functions are interpolated between original calculation points. The inclination of the correlation function in the gray scale plots shows the propagation direction of the perturbations, while the cut along a vertical line at $\tau=0$ gives the poloidal correlation length. Horizontal cuts at different poloidal positions give a correlation function whose maximum is shifted in τ. The location of the maximum indicates the propagation time to the given poloidal distance, which can be used for deducing the propagation velocity.

The left part of the figure shows correlation functions calculated from the simulated density fluctuations, while the right part shows results for the light fluctuations. As one can clearly see the poloidal correlation length is indeed affected, it becomes substantially longer for the light fluctuations than for the original density fluctuations. The temporal structure is not much affected in rows 1 and 2 where the poloidal flow velocity is constant. In contrast to this, in row 3, the radial integration effect of the beam is obvious: the light correlation function exhibits two maxima, each one corresponding to one of the velocities in the simulation. This effect is caused by the finite lifetime of the excited states in the Li beam where the correlation information is mixed in space to some extent. If one goes a little further into the plasma, the first peak disappears.

Figure 8 exaggerates the effect due to the sharp step in the poloidal flow velocity profile. In a smooth profile the effect is less obvious but it should be taken into account in the interpretation. As we know that the beam integration length is around 2–3 cm, changes in the poloidal correlation length and flow velocity over a 2 cm radial distance can be considered as real. For a given experimental situation one can check the smearing effect with the simulation. For a precise evaluation of the flow velocity and poloidal correlation length one would need a two-dimensional version of the reconstruction method described in Ref. 8.

IV. TWO-DIMENSIONAL LI-BEAM DIAGNOSTIC ON THE WENDELSTEIN 7-AS STELLARATOR

The original Li-beam diagnostic at the Wendelstein 7-AS stellarator[2] was upgraded to a two-dimensional setup and measurements with two virtual beams were performed. Additionally a series of measurements on identical plasmas with different amount of beam deflection were done and measurement of the full two-dimensional density profile, fluctuation correlation function and poloidal flow velocity was demonstrated.

Before measurements on the plasma, key elements of the deflection system were checked. First, beam deflection was tested with a static voltage applied across the 8-cm-long deflection plates separated by 4 cm. Beam shift was detected at a distance of approximately 1.5 m from the deflection plates by scanning its light emission in the residual gas by a rotating mirror. It was found that the beam could be moved without widening, as expected, if the voltage was applied symmetrically, that is, the same voltage with different polarity was applied onto the two deflection plates.

In the next step a high voltage switch circuitry was built and tested which is capable of switching up to 3 kV voltage within 100 ns on the deflection plates. The electrical connection scheme of the circuitry is shown in Fig. 9. A HTS-31-GSM high voltage transistor switch from Behlke Electronic GmbH is the centerpiece of the setup. It can switch up to 3 kV, and with sufficiently large buffer capacitors ($C_{b,1}$ and $C_{b,2}$) the device can be operated at 250 kHz frequency over several hundred ms. The switch can alternate a positive and a negative voltage on a deflection plate. The load resistors (R_1, R_2) and the buffer capacitors (C_1, C_2) were selected after the following considerations. R_1 is set to 50 Ω to limit the current through the electronic switch during short circuit or breakdown. As the C_L capacitance of the deflection plate and its associated cable is around 100 pF, the $R_1 C_L$ time constant is 5 ns, well below the needed 100 ns switch time. Buffer

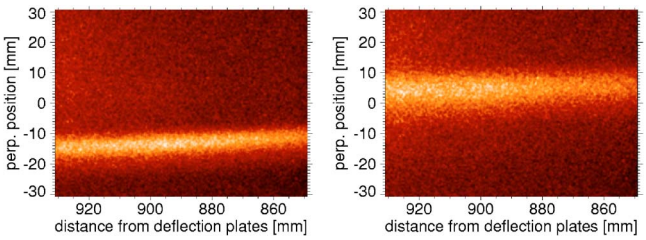

FIG. 10. Images acquired with the digital camera at 1 μs (left) and 5 μs (right) within the deflection period.

capacitor C_1 should be placed as close to the high voltage (HV) switch as possible and it should be a low-impedance type. Its value should be minimum 100 times C_L, in our case it was set to 600 nF.

Most of the current flowing from the HV power supplies is needed for periodically charging the C_L load capacitance to $\pm(U_1+U_2)$ voltage, thus for f switching frequency it is

$$I_{\mathrm{HV}} = C_L(U_1 + U_2)f. \tag{4.1}$$

For $U_1=U_2=1000$ V and $f=200$ kHz one gets 40 mA. We had HV power supplies with maximum 5 mA output current at hand, therefore the C_2 capacitor banks had to be added to preclude too large voltage drop during the few hundred ms operation time in one plasma discharge. $C_2=700$ μF was used which ensures that the voltage drop is less than 3% during 0.5 s operation. The C_2 capacitor banks can be recharged through the $R_2=5$ kΩ resistors in a few minutes between plasma discharges. The diodes on the output of the HV switch serve to protect the switch against overvoltage caused by the beam touching the deflection plate. A careful layout of grounding connections proved to be essential for noise protection.

The control signal of the HV switch and sampling signals for analog-to-digital (ADC) or image exposure by camera are derived from a common 10 MHz clock. A programmable divider generates a square wave for the HV switch. A second divider provides a separate train of pulses within each period of the HV switching. The frequency and phase of these pulses can be changed, this way the number and timing of samples or images in one deflection period can be set. The control signal of the HV switch was sampled in an ADC for reference.

Beam deflection was tested first by driving only one deflection plate with the HV switch and keeping the other at a fixed voltage. Although this causes some widening of the beam, it is fully appropriate for measuring the timing of the system. The light emitted by the Li beam by collisions with residual gas atoms in the flight tube was measured 90 cm from the deflection plates by a "SensiCam" fast shutter digital camera from PCO Optics GmbH. This camera can perform multiple exposures onto the same image. The beam was moved between two positions with a frequency of 100 kHz, that is it stayed at each position for 5 μs. The camera exposed for 1 μs always at the same time in the 10 μs deflection period. By exposing about 10^5 exposures onto the same image the faint beam light could be measured as is shown in Fig. 10. By moving the time of the exposure over the deflection period on a shot-to-shot basis, the beam position as a function of time could be determined with 1 μs resolution. The result in Fig. 11 shows that the beam can indeed be moved from one position to the other in less than 1 μs time. This result might seem to be trivial by considering the flight of the beam ions only. However, in reality the beam always contains some electrons attracted from the surrounding into

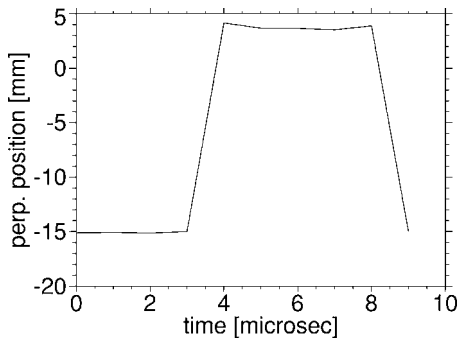

FIG. 11. Beam vertical position calculated from images taken at 1 μs time steps within the 10 μs beam deflection period.

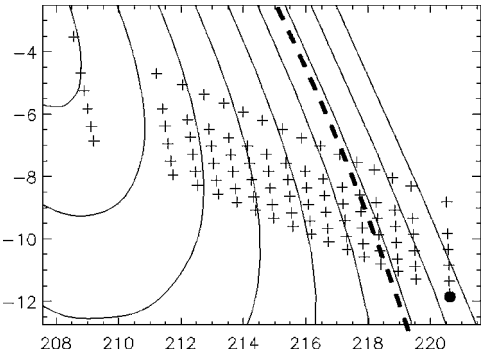

FIG. 12. Measurement grid in the (R,Z) coordinate space of W7-AS as determined by the crossing point of the 16 sightlines and the six virtual beam positions. The beam enters the plasma from the right side, the solid dot marks the outermost channel in the undeflected (reference) position. Shown detection channels are identical to the ones in Fig. 13; channel numbering increases from the plasma edge. The magnetic flux contours are overlain for reference, the dashed line indicates the position of the last closed flux surface.

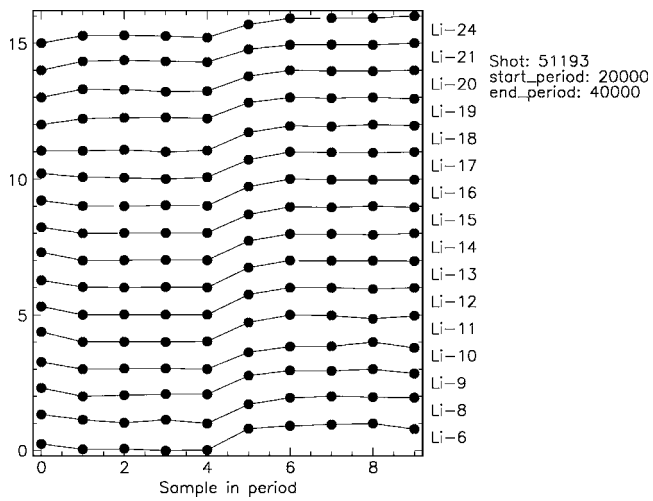

FIG. 13. Signals averaged over a deflection period and normalized between maximum and minimum.

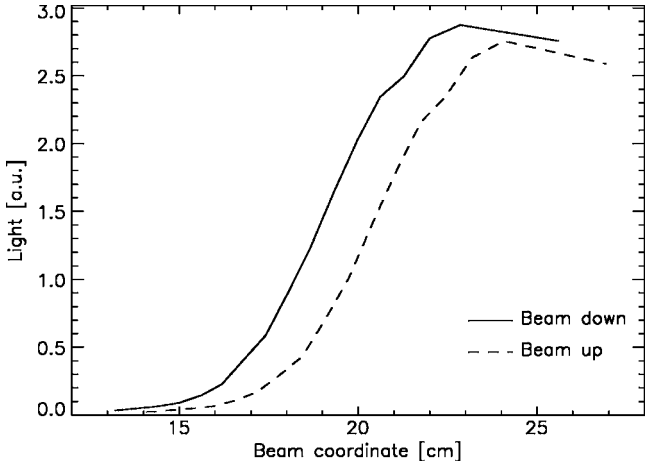

FIG. 14. Light profiles averaged over samples 1,2,3 (dashed) and 6,7,8 (solid) of the deflection period. The horizontal coordinate is moving with the beam, therefore a fixed position does not correspond to one observation channel.

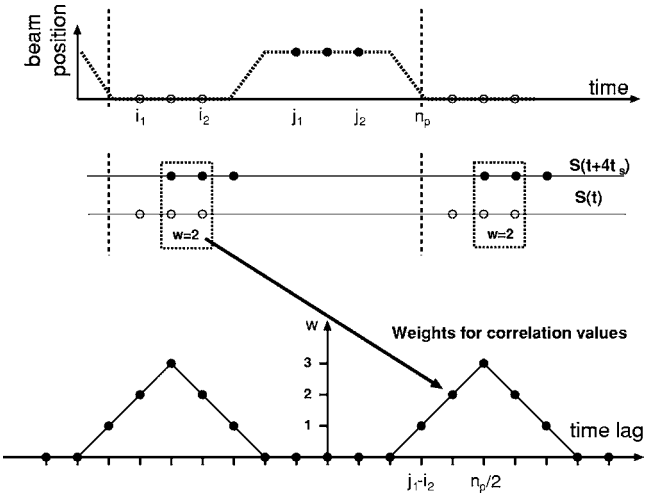

FIG. 16. Sampling times in one signal (top) and statistical weight of correlations at different time lags (bottom). Sampling is done equidistantly in time with t_s resolution. Samples i_1-i_2 are measured at one beam position, while j_1-j_2 are at the other. The vertical dashed lines indicate one deflection period. The figure in the middle explains how the w statistical weight at $\tau=4t_s$ is determined.

the beam by its space charge and it was not clear whether these electrons will play a role in beam movement.

Having tested the timing of beam movement a two virtual beam setup was built. The HV switch circuitry shown in Fig. 9 was duplicated for the second plate and the two circuits were operated in a 180° relative phase. Using four HV power supplies the voltage on the plates was alternated between $[-U_1,+U_1]$ and $[-U_2,+U_2]$; this way the beam was always deflected by symmetrical voltages. In this setup the beam is never switched off and the background light cannot be measured. To allow the determination of the background light long stationary discharges were used and at the end of the discharge the beam was completely removed from the plasma for about 100 ms by switching one of the deflection plates to a high voltage by a conventional relay. The light collected by the optics in this period of time was subtracted as background.

V. PROOF OF PRINCIPLE EXPERIMENTS

In the proof of principle experiment series six identical discharges were done. The U_1 voltage was set to 0; this defined a reference (undeflected) beam position. U_2 was changed from shot to shot through the values of 0, 50, 100, 150, 200 and 300. The beam position for these deflection voltages was measured before the experiments. A camera was placed to a window close to the point where the beam enters the plasma and an image was taken with static deflection at different deflection voltages. From these images the deflection as a function of voltage was determined and the beam position in the observation volume in the plasma was calculated. Sixteen channels were selected out of the 28 optical channels looking at the beam and they were sampled by the above described sampling method in 12 bit resolution ADC channels. The two-dimensional measurement grid resulting from the crossing point of the 16 sightlines and the six virtual beam positions is shown in Fig. 12.

In the experiments described in this section the beam was moved between the two positions with a period time of 10 μs and the signals were sampled with 1 MHz sampling rate, that is ten samples were taken in one period. As one can see from Fig. 12 the crossing point of the observation and the beam in most cases does not move along a magnetic flux surface; this way the density, and consequently the beam light intensity, changes in one channel when the beam moves from the reference position to the deflected one. This change cannot be directly observed in the signals, as due to the faint light the photon statistical noise is 10%–100%, but can be revealed by averaging the samples with the same timing within the deflection period over many periods. Figure 13 shows all 16 signals averaged and normalized between minimum and maximum. This figure gives the possibility of checking the timing of the measurement. As the signal amplifiers have a finite bandwidth, the signals cannot follow instantaneously the fast movement of the beam. After the

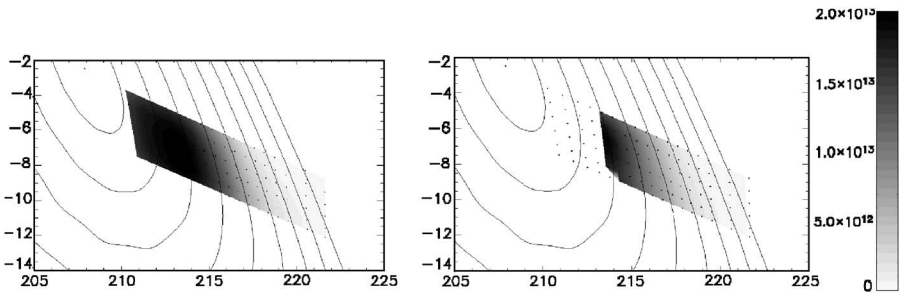

FIG. 15. Two-dimensional beam light profile (left) and plasma electron density profile constructed from a series of identical discharges with different beam deflection. The polidal flux contours from equilibrium calculation are shown for reference. The small dots indicate the measurement grid.

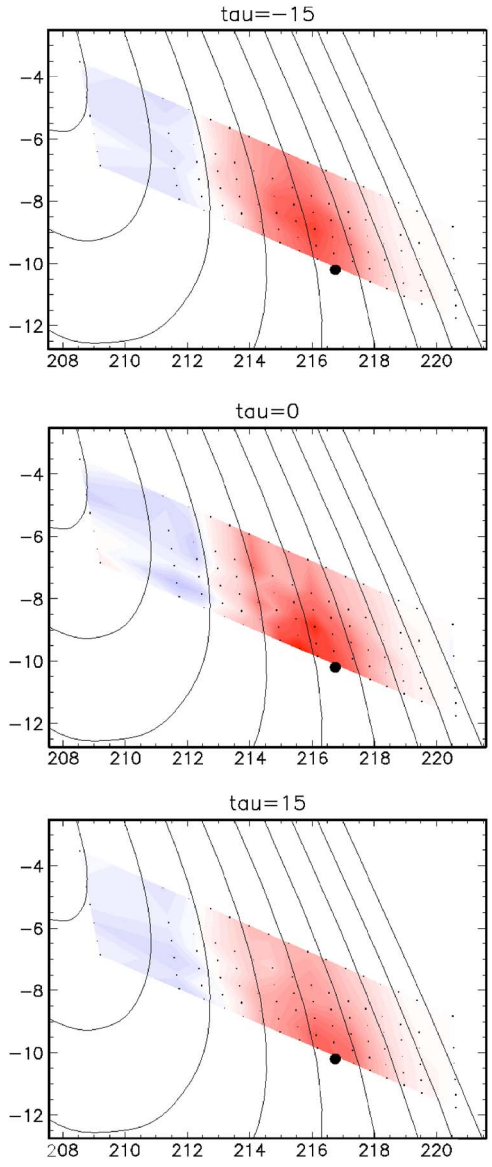

FIG. 17. Two-dimensional spatial covariance of density fluctuations at three different time lags: −15, 0+15 μs, from top to bottom. The small dots show the measurement points, the big dot is the reference position.

beam jumps from one position to another there is a certain time interval in which the signals carry information from both positions. These time intervals cannot be used for data evaluation. In Fig. 13 one can clearly see that samples 1,2,3 and 6,7,8 can be used for data evaluation; the other four samples should be dropped. From these samples in the periods one can construct two average beam light profiles along the two virtual beams as shown in Fig. 14. The expected shift in the profiles is well seen.

Such one-dimensional beam light profiles can be used for calculating the plasma electron density profile along the beam the same way as in the one-dimensional case.[3] From profiles calculated from discharges with different beam deflection, a two-dimensional beam light and electron density profile can be constructed as shown in Fig. 15. The reconstructed density profile appears to be constant along the flux surfaces as is expected from the huge difference in the $B_{\|}$ and $B\perp$ particle diffusion coefficient.

The evaluation of the fluctuation covariance functions (correlation function without normalization) from the measurement follows the principles laid down in Sec. II but more care is taken to extract the most information from the signals. The procedure is explained in Fig. 16. Within each deflection period the light signals are sampled between i_1 and i_2 when the beam is at one position and at j_1 and j_2 when it is at the other. The number of samples in one deflection period is n_p and we assume that the deflection is symmetrical in time: $i_2-i_1=j_2-j_1$. The cross-covariance function between the signal in the two beam positions can be calculated at each integer multiple of the t_s sampling time but there will be a different number of samples available at different τ time lags. This is indicated by the plot in the middle for $\tau=4t_s$. At this time lag the sampling points of $S(t)$ and $S(t+\tau)$ overlap at two places, therefore $w=2$. Generally at $0\leqslant\tau<(j_1-i_2)t_s$ and $(j_2-i_1)t_s<\tau<n_pt_s$ there is no correlation information ($w=0$), at $\tau=n_p/2t_s$ $w=i_2-i_1$ and in between w changes linearly in τ as shown in the figure. As a result we have correlation values at a series of points in one deflection period, but the w statistical weight (number of samples) is different for each τ. It is desirable to perform a binning procedure along the τ axis of this covariance function with a binning length equal to n_p. Averaging is done by taking into account the statistical weight of covariance values

$$\bar{C}[(jn_p+n_p/2)t_s]=\frac{\sum_{i=jn_p+1}^{jn_p+n_p} w_iC_i}{\sum_{i=jn_p+1}^{jn_p+n_p} w_i}. \tag{5.1}$$

The resulting covariance function will have a resolution n_p times the sampling time (10 μs in the actual experiment) and all correlation values will have equal statistical weight. To

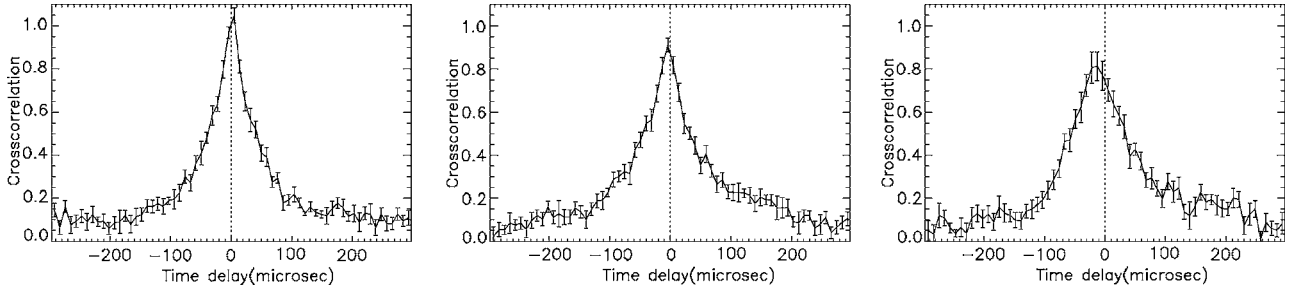

FIG. 18. Correlation function of beam light fluctuations along a flux surface for different displacements. Left: 0 displacement, channels 13-13; middle: 1 cm displacement, channels 13-13; right: 2 cm displacement, channels 13, 14.

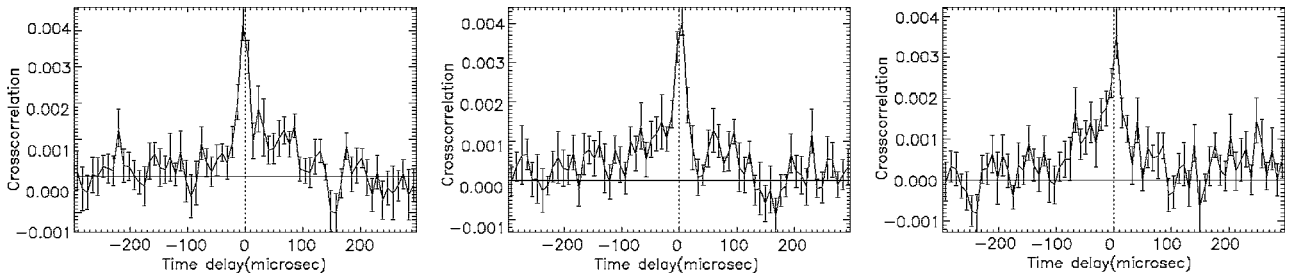

FIG. 19. Covariance function of beam light fluctuations along a flux surface at channel 18 for different displacements: 0, 1 and 2 cm, from left to right.

calculate the covariance function within one virtual beam on the same time lag scale a zero deflection measurement was used.

Using the above procedure a true three-dimensional covariance function can be constructed from the series of measurements in identical plasmas with different beam deflection. For each measurement point along the reference beam position the covariance to any point along and across the beam (2D spatial correlation) can be deduced with arbitrary τ time lag. From the covariance the correlation function could be calculated by dividing it with the fluctuation rms amplitudes. This is not always useful as at the edges of the profile, where the density drops, the fluctuation amplitude drops as well and the division with a rms value close to zero produces unreliable correlation values. This way in 2D plots of the correlation functions we use covariance functions, while in some other cases correlation functions are used.

Two-dimensional covariance functions in the Wendelstein 7-AS plasma around the last closed flux surface (LCFS) are shown in Fig. 17 at three different time lags. From these figures one can read several quantities which are in agreement with previous Langmuir probe and laser blow-off measurements:[9,17] the correlation length is around 1–2 cm both in the radial and poloidal direction. From the pictures at different time lags one can also read the propagation velocity of the turbulence: it is directed downwards in the plot, which corresponds to ion diamagnetic drift direction.

The flow velocity can be more exactly determined by plotting the correlation between a reference position and a series of measurement positions along the same flux surface as a function of time lag. For the reference point in Fig. 17 (channel 13) this is shown in Fig. 18. The measurement point should be displaced from the reference position only to that extent that a substantial correlation is seen. Correlation functions were used for this plot because the fluctuation amplitude could be well approximated for these positions and thus the covariance functions could be normalized.

The figure clearly shows that at 0 displacement the correlation function is approximately symmetric. (It is not completely symmetric as the autocorrelation is deduced from a 0 displacement measurement and not from the autocorrelation of one signal.) The maximum of the correlation function gradually shifts towards negative time lags with longer displacement. At 2 cm displacement the time shift is approximately 15 μs; this way the flow velocity is found to be 1300 m/s.

As previous one-dimensional measurements showed characteristics very similar to Langmuir probe measurements, we also tried to reproduce the flow reversal (shear layer) around the LCFS where the poloidal flow velocity reverses. This is made difficult by the fact that both the fluctuation relative amplitude and correlation time drop quickly inside the LCFS and smearing due to the lifetime of the Li excited states hindering good spatial resolution. Nevertheless, inside the LCFS some fluctuations can still be detected. Figure 19 shows three covariance functions at different displacements at channel 18. For these plots covariance functions were used as the approximation of the autopower became very inaccurate due to the short correlation time. The shift of the maximum covariance is definitely not the same as in the case of Fig. 18. It is somewhat on the positive side, indicating flow in the electron diamagnetic drift direction.

In the presented proof of principle experiments only 10 μs resolution was achieved for the correlation function, but the beam deflection technique has already been tested down to 4 μs resolution. However, to make use of the faster measurement it would be desirable to increase the equivalent current of the Li beam from the present 2 mA into the 5–10 mA range. Such efforts are under way.

ACKNOWLEDGMENTS

The authors from KFKI-RMKI would like to thank IPP-Garching for supporting this work in the framework of an RMKI-IPP collaboration contract.

[1] A. Huber, A. V. Nedospasov, U. Samm, and B. Schweer, J. Nucl. Mater. **266–269**, 546 (1999).
[2] G. K. McCormick, S. Fiedler, G. Kocsis, J. Schweinzer, and S. Zoletnik, Fusion Eng. Des. **34–35**, 125 (1996).
[3] J. Schweinzer, E. Wolfrum, F. Aumayr, M. Pöckl, H. Winter, R. P. Schorn, E. Hintz, and A. Unterreiter, Plasma Phys. Controlled Fusion **34**, 1173 (1992).
[4] D. M. Thomas, Rev. Sci. Instrum. **66**, 806 (1995).
[5] A. Komori, O. Mitarai, K. Yamagiwa, C. Honda, K. Kadota, J. Fujita, Y. T. Lie, U. Samm, A. Pospieszczyk, K. Hötkher, P. Bogen, and E. Hintz, Nucl. Fusion **28**, 1460 (1988).
[6] R. J. Fonck, G. Cosby, R. D. Durst, S. F. Paul, N. Bretz, S. Scott, E. Synakowski, and G. Taylor, Phys. Rev. Lett. **70**, 3736 (1993).
[7] R. J. Fonck, P. A. Duperrex, and S. F. Paul, Rev. Sci. Instrum. **61**, 3487 (1990).
[8] S. Zoletnik, S. Fiedler, G. Kocsis, G. K. McCormick, J. Schweinzer, and H. P. Winter, Plasma Phys. Controlled Fusion **40**, 1399 (1998).
[9] M. Endler, L. Giannone, K. McCormick, H. Niedermeyer, A. Rudyj, G. Theimer, N. Tsois, and S. Zoletnik, Phys. Scr. **51**, 610 (1995).
[10] S. J. Zweben and R. W. Gould, Nucl. Fusion **25**, 171 (1985).
[11] C. Hidalgo, J. H. Harris, T. Uckan, J. D. Bell, B. A. Carreras, J. L. Dunlap, G. R. Dyer, C. P. Ritz, A. J. Wootton, M. A. Meier, T. L. Rhodes, and K. Carter, Nucl. Fusion **31**, 1471 (1991).
[12] Yu. Y. Karzhavin, R. D. Durst, R. D. Bengston, R. V. Bravenec, D. L. Brower, G. Cima, R. J. Fonck, J. W. Heard, J. S. Kim, A. N. Nikitin, A. Ouroua, E. J. Powers, D. R. Roberts, C. Watts, and A. J. Wootton, in *22rd*

EPS Conference on Controlled Fusion and Plasma Physics, Bournemouth, 1995 (European Physical Society Mulhouse, Europhys. Conf. Abstracts Vol. 19C) IV-097 (1995).
[13] A. Huber, PhD. thesis, Heinrich-Heine-Universität, Düsseldorf.
[14] S. Zoletnik, M. Anton, M. Endler, S. Fiedler, M. Hirsch, K. McCormick, J. Schweinzer and W7-AS Team, Phys. Plasmas **6**, 4239 (1999).
[15] S. Zoletnik, G. Kocsis, S. Fiedler, K. McCormick, J. Schweinzer, W7-AS Team and H. P. Winter, IPP-Garching Report No. IPP III/213 (1996).
[16] H. Thomsen, M. Endler, J. Bleuel, A. V. Chankin, S. K. Erents, and G. F. Matthews, Phys. Plasmas **9**, 1233 (2002).
[17] M. Bruchhausen, R. Burhenn, M. Endler, G. Kocsis, A. Pospieszczyk, and S. Zoletnik; Plasma Phys. Controlled Fusion **46**, 489 (2004).